Accelerating spectral-based color separation within the Neugebauer subspace

Philipp Urban
Mitchell R. Rosen
Roy S. Berns
Rochester Institute of Technology
Chester F. Carlson Center for Imaging Science
Munsell Color Science Laboratory
54 Lomb Memorial Drive
Rochester, New York 14623
E-mail: urban@cis.rit.edu

Abstract. *Spectral separation is the process of obtaining printer control values to reproduce a given spectral reflectance. Given a multispectral image where each pixel represents a spectral reflectance, separation could be implemented by inverting a physical printer model on a pixel-by-pixel basis. Such a process would obviously need to be very fast to handle high-resolution images in a reasonable time. For a printer whose spectral response is characterized by the Yule–Nielsen spectral Neugebauer model, the linear regression iteration (LRI) method can be used to invert the model. We introduce the subspace linear regression iteration (SLRI) method, a modification of LRI shown to be significantly accelerated due to performing its calculations within the subspace determined by the Neugebauer primaries. Using this subspace approach, the number of multiplications becomes independent of the spectral sampling rate. Using a standard six color printer and a common spectral sampling rate, the number of multiplications can be decreased by about two-thirds without changing the convergence behavior.* [DOI: 10.1117/1.2805447]

1 Introduction

To reproduce multispectral images by a printer, suitable control values need to be calculated to minimize the distance to the original by means of a spectral metric. This process is called spectral separation. In contrast to traditional separation techniques, which try to adjust the print so that it matches the original for exactly one illuminant (e.g., ICC[1] using CIELAB), the main aim of spectral separation is to minimize the effect of metamerism for more than one illuminant. The match between the original and the reproduction should be invariant under illuminant changes. Unfortunately, printing devices are, in general, not able to reproduce most of the natural reflectances, so that spectral gamut mapping[2–4] is an important part and the first stage of the process. The second stage of spectral separation is the inversion of a spectral printer model representing a predicting function from control value space into reflectance space.

In recent years, various spectral printer models have been developed.[5] Many of them are extensions of the well-known Neugebauer model.[6] Due to its simplicity and accuracy, the Yule–Nielsen modified Neugebauer model[7,8] and its spectral expansion,[9,10] the Yule–Nielson spectral Neugebauer (YNSN) model, have become the most popular models and are widely used today for printer characterization. Unfortunately, an analytical inversion of the YNSN model is generally not possible, although several approaches have been proposed using iterative optimization techniques.[11–14] By utilizing the multilinearity of the YNSN model in $1/n$ space, the linear regression iteration (LRI) method[15] performs the inversion in terms of the minimal RMS error in $1/n$ space and uses only two matrix-vector multiplications for each iteration step.

For the spectral-based separation of high-resolution multispectral images, processing speed is one of the major considerations for practical applications. The goal of this paper is to investigate an approach to spectral model inversion that reduces the number of computations necessary to create an accurate separation for spectral reproduction enabling direct model inversion on a pixel-by-pixel basis. The number of multiply instructions needed for the LRI inversion of a YNSN model is decreased significantly without changing the convergence behavior by performing the iterations within the subspace determined by the Neugebauer primaries.

It is outside the scope of this paper to address the accuracy of the YNSN model for printers. Reference is made to Rolleston and Balasubramanian[16] and Wyble and Berns[5] for that purpose. Here, the inversion of the model is of interest. Thus, for the sake of the present discussion, the YNSN model will be considered to be accurate in its forward implementation for the printers in question.

1.1 *The Yule–Nielsen Spectral Neugebauer (YNSN) Model*

The YNSN[6–10] model is one of the most widely used models for the prediction of reflectance spectra produced by a printer. The important effect of optical dot gain is incorporated through the use of an empirical factor that can be derived using a relatively small number of measurements. Assuming a uniform distribution of the dots on the substrate, the general YNSN model for an m-colorant printer takes the form

Paper 06109R received Jun. 22, 2006; revised manuscript received Feb. 7, 2007; accepted for publication Jun. 26, 2007; published online Dec. 12, 2007.
1017-9909/2007/16(4)/043014/11/$25.00 © 2007 SPIE and IS&T.

Table 1 Example of the Demichel equations for a CMY printer.

i	$p(i,1)$	$p(i,2)$	$p(i,3)$	$a_i(\psi_c,\psi_m,\psi_y)$
1	0	0	0	$a_1(\psi_c,\psi_m,\psi_y)=(1-\psi_c)(1-\psi_m)(1-\psi_y)$
2	1	0	0	$a_2(\psi_c,\psi_m,\psi_y)=\psi_c(1-\psi_m)(1-\psi_y)$
3	0	1	0	$a_3(\psi_c,\psi_m,\psi_y)=(1-\psi_c)\psi_m(1-\psi_y)$
4	1	1	0	$a_4(\psi_c,\psi_m,\psi_y)=\psi_c\psi_m(1-\psi_y)$
5	0	0	1	$a_5(\psi_c,\psi_m,\psi_y)=(1-\psi_c)(1-\psi_m)\psi_y$
6	1	0	1	$a_6(\psi_c,\psi_m,\psi_y)=\psi_c(1-\psi_m)\psi_y$
7	0	1	1	$a_7(\psi_c,\psi_m,\psi_y)=(1-\psi_c)\psi_m\psi_y$
8	1	1	1	$a_8(\psi_c,\psi_m,\psi_y)=\psi_c\psi_m\psi_y$

$$R_\lambda(\vec{\psi})=\left[\sum_{i=1}^{2^m} a_i(\vec{\psi})R_{i,\lambda}^{1/n}\right]^n, \tag{1}$$

where $\vec{\psi}=(\psi_1,\ldots,\psi_m)^T$, $\psi_i\in[0,1]$, are the effective area coverages of the colorants (e.g., CMY), $R_{i,\lambda}$ are the Neugebauer primaries, n is the empirical Yule–Nielsen factor modeling the optical dot gain, and $a_i(\vec{\psi})$ are the Demichel equations

$$a_i(\vec{\psi})=\prod_{j=1}^{m}\psi_j^{p(i,j)}(1-\psi_j)^{1-p(i,j)}, \tag{2}$$

$$p(i,j)=\frac{\text{bitand}(2^{(j-1)},i-1)}{2^{(j-1)}}. \tag{3}$$

Mathematically, the Demichel equations are the weighting functions of the Neugebauer primaries used by multilinear interpolation. Table 1 shows an example for a CMY printer.

To use the YNSN model, the control values must be transformed initially to the effective area coverages performed in practice by one-dimensional lookup tables. A detailed description of the YNSN model including physical backgrounds is given in Refs. 17–20. Fitting techniques for the n-value and the calculation of the effective area coverages can be found in Ref. 21.

1.2 *The Linear Regression Iteration (LRI) Method*

To invert the YNSN model for an m-colorant printer by means of the minimal spectral RMS error for a given reflectance spectrum r_λ, the following constraint optimization problem has to be solved:

Minimize

$$\|R_\lambda(\vec{\psi})-r_\lambda\|_2^2 \tag{4}$$

with the constraint

$$\vec{\psi}\in[0,1]^m, \tag{5}$$

where $\|\ldots\|_2^2$ in Eq. (4) denotes the square of the 2-norm.

The LRI method[15] uses the discrete formulation of the problem by sampling the spectra at N wavelengths, so that each continuous spectrum is transformed into an N-dimensional vector. A typical sampling distance is 10 nm in the wavelength range of 400–700 nm,[22] resulting in $N=31$.

The LRI method utilizes the property of the YNSN model to be multilinear in $1/n$ space, i.e., for each ψ_i, the following decomposition of the YNSN model in $1/n$ space applies:

$$R_\lambda^{1/n}(\vec{\psi})=A_i(\vec{\psi})\cdot\psi_i+B_i(\vec{\psi}), \tag{6}$$

$$\frac{\partial A_i(\vec{\psi})}{\partial\psi_i}=\frac{\partial B_i(\vec{\psi})}{\partial\psi_i}=0. \tag{7}$$

Equation (7) is equivalent to the independence of $A_i(\vec{\psi})$ and $B_i(\vec{\psi})$ from ψ_i.

Setting the right side of Eq. (6) equal to the given reflectance $r_\lambda^{1/n}$ allows the optimal calculation of ψ_i in the sense of the minimal RMS error in $1/n$ space using simple linear regression:

$$\psi_i^{\min}=\frac{\vec{\mathrm{A}}_i^T(\vec{\psi})(\vec{\mathrm{r}}-\vec{\mathrm{B}}_i(\vec{\psi}))}{\vec{\mathrm{A}}_i^T(\vec{\psi})\vec{\mathrm{A}}_i(\vec{\psi})}, \tag{8}$$

where $\vec{\mathrm{A}}_i(\vec{\psi})$, $\vec{\mathrm{B}}_i(\vec{\psi})$, and $\vec{\mathrm{r}}\in\mathbb{R}^N$ are the discrete approximations of $A_i(\vec{\psi})$, $B_i(\vec{\psi})$, and $r_\lambda^{1/n}$. Iterating this equation by successively recalculating the ψ_i and considering the constraint in Eq. (5) leads to the LRI algorithm with starting point $\vec{\psi}=(\psi_1^0,\ldots,\psi_m^0)^T$:

```
1. REPEAT {
2.    FOR (i=1; i≤m; i=i+1)
3.    {
4.       ψ_i=Ā_1^T(ψ)(r̄−B̄_i(ψ))/(Ā_1^T(ψ)Ā_i(ψ));
5.       IF (ψ_i<0) {ψ_i=0};
6.       IF (ψ_i>1) {ψ_i=1};
7.    }
8. } UNTIL Termination
```

A detailed explanation of the convergence behavior of the LRI method is given in Urban and Grigat,[15] where recommendations for implementation can also be found.

1.3 *Termination Criteria*

The following criteria are proposed by Gill *et al.*[23] if it is desired that the value of the objective function at the point $\vec{\psi}^k$ agree with the first q decimal places of the real minimum:

C1: $F(\vec{\psi}^{k-m})-F(\vec{\psi}^k)\leq\tau(1+F(\vec{\psi}^k))$,
C2: $\|\vec{\psi}^{k-m}-\vec{\psi}^k\|\leq\sqrt{\tau}(1+\|\vec{\psi}^k\|)$,
C3: $k\geq k_{\max}$,

where $\tau:=10^{-q}$ and F is our discrete objective function, i.e.,

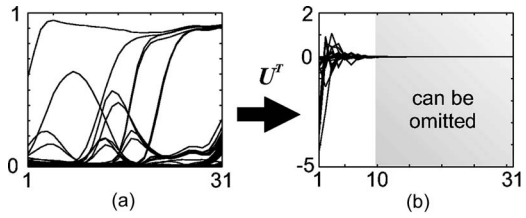

Fig. 1 (a) Usual Neugebauer primaries of a six-colorant printer. (b): The same Neugebauer primaries after the coordinate transform using the unitary matrix U^T.

$$F(\vec{\psi}) = \|\vec{\mathrm{R}}(\vec{\psi}) - \vec{\mathrm{r}}\|_2^2. \tag{9}$$

Here, $\vec{\mathrm{R}}(\vec{\psi})$ and $\vec{\mathrm{r}}$ are the discrete approximations of $R_\lambda^{1/n}(\vec{\psi})$ and $r_\lambda^{1/n}$. The iteration can be terminated when C1 *and* C2 are satisfied *or* when condition C3 occurs, where $k_{\max}$ is a user-defined maximum number of iteration steps.

1.4 *Complexity of the LRI Method*

Unlike many iterative optimization techniques, such as Newton-like methods, the LRI method requires neither an evaluation of the Jacobi or Hesse matrix nor a solution to a linear equation system. One iteration step consists mainly of two simple matrix-vector multiplications.

The number of multiplication operations $\mathcal{N}$ for each iteration of the LRI method is dependent on the number of colorants m and the spectral sampling rate N. The multiplications are needed to determine the regression term at line 4 of the algorithm. The majority of multiplications are necessary to calculate the vectors $\vec{\mathrm{A}}_i(\psi)$ and $\vec{\mathrm{B}}_i(\psi)$. These vectors can be calculated by multiplying a vector $\vec{\mathrm{v}}_i(\vec{\psi}) \in \mathbb{R}^{(2^{m-1})}$ with the $(N \times 2^{m-1})$-dimensional matrices A_i and B_i:

$$\vec{\mathrm{A}}_i(\vec{\psi}) = \mathrm{A}_i \vec{\mathrm{v}}_i(\vec{\psi}), \tag{10}$$

$$\vec{\mathrm{B}}_i(\vec{\psi}) = \mathrm{B}_i \vec{\mathrm{v}}_i(\vec{\psi}), \tag{11}$$

where $\vec{\mathrm{v}}_i(\vec{\psi}) = (\mathrm{v}_i^1(\vec{\psi}), \ldots, \mathrm{v}_i^{2^{m-1}}(\vec{\psi}))^T$ and

$$\mathrm{v}_i^k(\vec{\psi}) = \prod_{j=1}^{m-1} \psi_{i_j}^{p(k,j)}, \quad i_j = \begin{cases} j, & j < i, \\ j+1, & j \geq i. \end{cases} \tag{12}$$

A_i and B_i are not dependent on the effective area coverages and can be determined once by simply expanding and rearranging the YNSN model. An example of the matrices A_i and B_i and the vector $\vec{\mathrm{v}}_i(\vec{\psi})$ is given in the Appendix.

The calculation of $\vec{\mathrm{v}}_i(\vec{\psi})$ has to be performed for each iteration and needs $(2^{m-1}-m)$ multiplications; the calculation of the matrix-vector multiplications in Eqs. (10) and (11) needs $N \cdot 2^{m-1}$ each. In addition, $2N$ multiplications are necessary to calculate the two scalar products $\vec{\mathrm{A}}_i^T(\vec{\psi})(\vec{\mathrm{r}} - \vec{\mathrm{B}}_i(\vec{\psi}))$ and $\vec{\mathrm{A}}_i^T(\vec{\psi})\vec{\mathrm{A}}_i(\vec{\psi})$ in Eq. (8). The total number of multiplications cumulates to

$$\mathcal{N}(N,m) = (2^{m-1} - m) + N \cdot 2^m + 2N. \tag{13}$$

For an $m=6$ colorant printer and a spectral sampling rate of $N=31$, each iteration step of the LRI method needs

$$\begin{aligned} \mathcal{N}(31,6) &= (2^{6-1} - 6) + 31 \cdot 2^6 + 2 \cdot 31 \\ &= 30 + 1984 + 62 = 2072 \end{aligned} \tag{14}$$

multiplications. This seems like a lot but should be viewed in relation to the calculation of the forward YNSN model that needs $(2^{m-1}-m)+N \cdot 2^m + N = 2041$ multiplications if calculated according to Eq. (6).

The majority of multiplications has to be performed for calculating the matrix-vector multiplications in Eqs. (10) and (11). Performing the iteration within the subspace defined by the Neugebauer primaries reduces the row dimension of the matrices and therefore the number of required multiplications drastically without changing the convergence behavior. In the next section, the concept of the subspace calculation is presented and the minor changes on the LRI method are described.

2 The Subspace Approach

The spectral gamut of usual printers is low in dimension compared to the whole spectral space. On the one hand, this seems to be a drawback since multispectral images cannot be reproduced generally in an error-free way and spectral

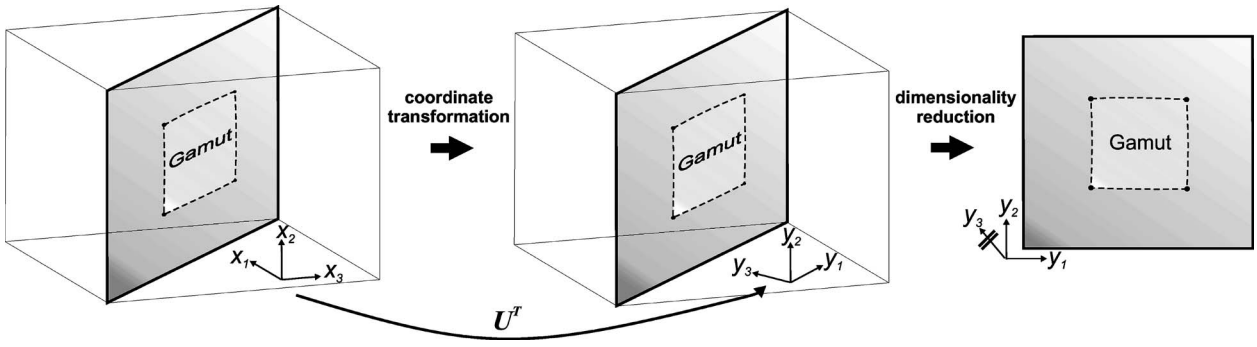

Fig. 2 Schematic visualization of the subspace approach: Multiplying with U^T transforms the coordinate system. Reducing the dimensionality to K does not change the accuracy.

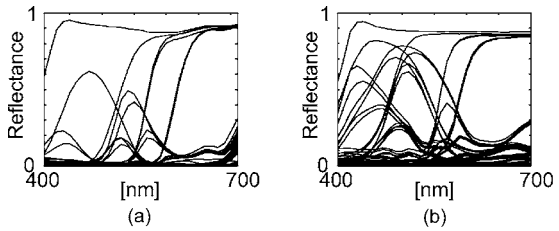

Fig. 3 Neugebauer primaries used in simulation experiments. (a) Canon i9900 dye-based inkjet printer using six inks (cyan, magenta, yellow, black, red, and green) on Canon Photo Paper Pro (PR-101). (b) Epson Stylus Pro 5500 pigment-based inkjet printer using six inks (cyan, magenta, yellow, black, orange, and green) on Epson photo-quality glossy paper (KA3N20MDK).

Fig. 4 The multispectral images used in Simulation II transformed in sRGB: (a) *Young Girl* 147×87 pixels; (b) *Fruits and Flowers* 120×160 pixels.

gamut mapping transformations are necessary. On the other hand, this is a large advantage for saving computational effort.

The new subspace approach is based on the length-preserving properties of unitary transformations, i.e., if X is a real-valued, unitary matrix ($X^TX=XX^T=I$) and $\vec{x}$ is a vector, the following equation applies:

$$\|X\vec{x}\|_2 = \sqrt{(X\vec{x})^T(X\vec{x})} = \sqrt{\vec{x}^TX^TX\vec{x}} = \sqrt{\vec{x}^T\vec{x}} = \|\vec{x}\|_2. \tag{15}$$

If we apply this to the discrete form of the objective function (4) in $1/n$ space, we can multiply the difference spectrum with each real-valued, unitary matrix X without changing the function values:

$$\|\vec{\mathrm{R}}(\vec{\psi}) - \vec{\mathrm{r}}\|_2^2 \overset{(15)}{=} \|X(\vec{\mathrm{R}}(\vec{\psi}) - \vec{\mathrm{r}})\|_2^2 \tag{16}$$

$$= \|X\mathrm{R}\vec{\mathrm{a}}(\vec{\psi}) - X\vec{\mathrm{r}}\|_2^2, \tag{17}$$

where $\vec{\mathrm{r}}=(r_{\lambda_1}^{1/n},\ldots,r_{\lambda_N}^{1/n})^T$ is the discretized reflectance spectrum in $1/n$ space, $\vec{\mathrm{R}}(\vec{\psi})=(R_{\lambda_1}(\vec{\psi})^{1/n},\ldots,R_{\lambda_N}(\vec{\psi})^{1/n})^T$ is the discretized YNSN predicted spectrum in $1/n$ space, $\mathrm{R}=(\vec{\mathrm{R}}_1,\ldots,\vec{\mathrm{R}}_{2^m})$ is the matrix of the Neugebauer primaries raised to the power of $1/n$, i.e., $\vec{\mathrm{R}}_i=(R_{i,\lambda_1}^{1/n},\ldots,R_{i,\lambda_N}^{1/n})^T$, and $\vec{\mathrm{a}}(\vec{\psi})=(a_1(\vec{\psi}),\ldots,a_{2^m}(\vec{\psi}))^T$ is the vector of the Demichel equations defined in Eq. (2).

The real-valued, unitary matrix X performs an orthonormal basis transformation of the spectral space. If we can find a matrix X that transforms the basis of the spectral space in a way that a small number of the new basis vectors span the subspace effectively defined by the Neugebauer primaries, the remaining dimensions can be omitted, since they are not affected by the YNSN model (see Figures 1 and 2).

This matrix can easily be found by a singular-value decomposition of the matrix R:

$$\mathrm{R} = USV^T, \tag{18}$$

where the real-valued, unitary matrix $U=(\vec{u}_1,\ldots,\vec{u}_N)$ contains the characteristic spectra of the Neugebauer primaries as column vectors sorted according to their variances (or singular values), which are the diagonal elements of the matrix S. The singular values are sorted in descending order, i.e., $s_i \geqslant s_{i+1}$, and for common printers only few are significantly larger than zero. The column vectors of U, which belong to these K singular values, $K \ll N$, span the subspace effectively defined by the Neugebauer primaries. If the sampling rate is larger than the number of Neugebauer primaries, i.e., $N>2^m$, we extend, without changing the matrix R, the $(N\times 2^m)$-dimensional matrix S and the $2^m\times 2^m$ real-valued, unitary matrix V^T by zero values, so that S becomes an $(N\times N)$-dimensional matrix and V^T an $(N\times 2^m)$-dimensional matrix. We denote the whole diagonal elements of S by s_i, so that for $N>2^m$, $s_i=0$, $i>2^m$.

To transform the coordinates of the spectral space consistent with the Neugebauer subspace, we have to set (see Fig. 1)

$$X := U^T. \tag{19}$$

Inserting Eq. (19) into Eq. (17) results in

$$\|\vec{\mathrm{R}}(\vec{\psi}) - \vec{\mathrm{r}}\|_2^2 \overset{(17)(19)}{=} \|U^T\mathrm{R}\vec{\mathrm{a}}(\vec{\psi}) - U^T\vec{\mathrm{r}}\|_2^2 \tag{20}$$

$$\overset{(18)}{=} \|SV^T\vec{\mathrm{a}}(\vec{\psi}) - U^T\vec{\mathrm{r}}\|_2^2 \tag{21}$$

$$= \sum_{i=1}^{K} (s_i\vec{v}_i^T\vec{\mathrm{a}}(\vec{\psi}) - \vec{u}_i^T\vec{\mathrm{r}})^2 + \sum_{i=K+1}^{N} \underbrace{(s_i\vec{v}_i^T\vec{\mathrm{a}}(\vec{\psi})}_{\approx 0} - \vec{u}_i^T\vec{\mathrm{r}})^2 \tag{22}$$

$$\approx \sum_{i=1}^{K} (s_i\vec{v}_i^T\vec{\mathrm{a}}(\vec{\psi}) - \vec{u}_i^T\vec{\mathrm{r}})^2 + \sum_{i=K+1}^{N} (\vec{u}_i^T\vec{\mathrm{r}})^2. \tag{23}$$

In Eq. (22), the term $s_i\vec{v}_i^T\vec{\mathrm{a}}(\vec{\psi})$ in the second sum can be neglected because $s_i \approx 0$, $\|\vec{\mathrm{a}}(\vec{\psi})\|_1 \leqslant 1$, and the matrix V^T is unitary, i.e., $\|\vec{v}_i\|_2=1$ (or in the case of $N>2^m$, $\vec{v}_i=0$, $i>2^m$ as set above).

Since we are interested in the effective area coverages $\vec{\psi}$ that minimize the objective function, we can omit the second sum in Eq. (23) because it is independent of $\vec{\psi}$.

Therefore, the solution of the discretized minimization problem (4) and (5) in $1/n$ space is approximately the same as the solution of the following optimization problem:

Table 2 RMS results for Simulation I. For each *K*, the mean, standard deviation, and maximal RMS error and the average number of iterations were calculated for all Yule–Nielsen *n*-values. A *K* value of 31 is similar to the plain LRI method.

	Canon				Epson			
	RMS			Iterations	RMS			Iterations
K	Mean	Std	Max	Mean	Mean	Std	Max	Mean
1	0.148	0.231	2.457	11.9	0.227	0.273	2.430	11.9
2	0.073	0.106	1.515	19.9	0.116	0.145	1.398	16.5
3	0.038	0.046	0.900	30.1	0.058	0.076	1.006	34.0
4	0.027	0.031	0.709	55.2	0.026	0.025	0.305	62.7
5	0.023	0.026	0.272	62.4	0.022	0.018	0.169	73.5
6	0.017	0.020	0.205	74.0	0.021	0.018	0.169	74.7
7	0.014	0.018	0.204	79.4	0.020	0.017	0.167	76.7
8	0.012	0.015	0.204	83.3	0.019	0.016	0.141	84.6
9	0.012	0.015	0.195	84.7	0.018	0.015	0.141	85.5
10	0.011	0.015	0.195	86.2	0.018	0.015	0.140	85.7
11	0.011	0.014	0.195	87.0	0.018	0.015	0.140	87.3
⋮	⋮	⋮	⋮	⋮	⋮	⋮	⋮	⋮
31	0.011	0.014	0.195	88.6	0.018	0.015	0.140	87.9

$$\|U_K^T\vec{\mathrm{R}}(\vec{\psi}) - U_K^T\vec{\mathrm{r}}\|_2^2 \overset{!}{=} \min \tag{24}$$

with the constraint

$$\vec{\psi} \in [0,1]^m, \tag{25}$$

where $U_K^T=(\vec{u}_1,\ldots,\vec{u}_K)^T$ is the matrix containing the first K most significant characteristic spectra of the Neugebauer primaries.

2.1 *Determination of K*

Since the Demichel equations $\vec{\mathrm{a}}(\vec{\psi})=(a_1(\vec{\psi}),\ldots,a_{2^m}(\vec{\psi}))^T$ satisfy $\Sigma a_i(\vec{\psi})=1$, $a_i(\vec{\psi})\geqslant 0$, and $\forall i\in\{1,\ldots,2^m\}\exists\,\vec{\psi}\in[0,1]^m: a_i(\vec{\psi})=1$, and V in Eq. (18) is unitary, the following equation applies:

$$\max_{\vec{\psi}}|\vec{v}_i^T\vec{\mathrm{a}}(\vec{\psi})| = \max_j|v_{ij}| =: v_i^{\max} \leqslant 1. \tag{26}$$

After defining an application dependent threshold T, describing the maximal acceptable difference of predicted and given reflectance in $1/n$ space, K can be chosen as follows:

$$K = \min\left\{ j\in\{1,\ldots,N\} \middle| \sum_{i=j}^{N} s_i v_i^{\max} \leqslant T \right\}. \tag{27}$$

2.2 *Revision of the LRI Method*

The new algorithm has the following form with starting point $\vec{\psi}=(\psi_1^0,\ldots,\psi_m^0)^T$:

```
1. REPEAT {
2.     FOR (i=1; i⩽m; i=i+1)
3.     {
4.         ψ_i=(U_K^T Ā_i(ψ⃗))^T (U_K^T r⃗ − U_K^T B̄_i(ψ⃗))/
               ((U_K^T Ā_i(ψ⃗))^T (U_K^T Ā_i(ψ⃗)));
5.         IF (ψ_i<0) {ψ_i=0};
6.         IF (ψ_i>1) {ψ_i=1};
7.     }
8. } UNTIL Termination
```

According to Eqs. (10) and (11), the multiplications with U_K^T can be calculated in advance, i.e.,

$$U_K^T\vec{\mathrm{A}}_i(\vec{\psi}) = U_K^T(\mathrm{A}_i\vec{\mathrm{v}}_i(\vec{\psi})) = (U_K^T\mathrm{A}_i)\vec{\mathrm{v}}_i(\vec{\psi}), \tag{28}$$

$$U_K^T\vec{\mathrm{B}}_i(\vec{\psi}) = U_K^T(\mathrm{B}_i\vec{\mathrm{v}}_i(\vec{\psi})) = (U_K^T\mathrm{B}_i)\vec{\mathrm{v}}_i(\vec{\psi}), \tag{29}$$

where $U_K^T\mathrm{A}_i$ and $U_K^T\mathrm{B}_i$ are $(K\times 2^{m-1})$-dimensional matrices.

We denote the new algorithm the *subspace linear regression iteration* (SLRI).

Table 3 Colorimetric results for the Canon printer in Simulation I. For each K, the mean, standard deviation, and maximal ΔE_{00}-values were calculated for all Yule–Nielsen n-values. A K value of 31 is similar to the plain LRI method.

	ΔE_{00}, A			ΔE_{00}, C			ΔE_{00}, F11		
K	Mean	Std	Max	Mean	Std	Max	Mean	Std	Max
1	12.1	9.2	62.8	12.3	8.7	75.5	12.7	9.2	75.7
2	8.1	6.8	61.1	9.9	7.8	72.5	10.2	8.1	73.1
3	2.0	2.4	29.4	2.0	2.2	26.4	2.7	3.1	34.1
4	1.6	2.4	30.1	1.4	2.1	27.8	2.1	2.8	34.7
5	1.3	2.0	26.4	1.1	1.5	20.0	1.8	2.3	28.8
6	1.0	1.6	25.6	0.8	1.2	18.5	1.3	1.8	27.0
7	0.7	0.9	18.8	0.7	0.8	13.9	1.0	1.2	19.6
8	0.6	0.5	13.6	0.6	0.5	11.7	0.8	1.0	18.9
9	0.6	0.5	13.4	0.5	0.5	12.2	0.8	0.8	19.2
10	0.5	0.4	13.4	0.5	0.4	12.1	0.8	0.8	19.1
11	0.5	0.4	13.4	0.5	0.4	12.1	0.8	0.8	19.1
⋮	⋮	⋮	⋮	⋮	⋮	⋮	⋮	⋮	⋮
31	0.5	0.4	12.3	0.5	0.4	11.9	0.7	0.7	19.0

2.3 *Complexity Estimation*

We quantify the complexity of the SLRI method in terms of multiplication operations for each iteration step. The multiplication of U_K^T with A_i and B_i can be performed just once and in advance [see Eqs. (28) and (29)]. Also the multiplication of U_K^T with $\vec{r}$ can be performed just once for each given reflectance spectrum. Hence, the resulting number of multiplications for each iteration step is equivalent to Eq. (13), when we replace the spectral rate N by the effective dimension of the Neugebauer subspace K, i.e.,

$$\mathcal{N}(K,m) = (2^{m-1} - m) + K \cdot 2^m + 2K. \tag{30}$$

Using a common $m=6$ printer, the effective dimension can usually be chosen as $K=9$, and the number of multiplications is

$$\mathcal{N}(9,6) = (2^{6-1} - 6) + 9 \cdot 2^6 + 2 \cdot 9 = 620, \tag{31}$$

that is, only 30% of the multiplications needed for each iteration step of the LRI method; see Eq. (14).

3 Experiments

The aim of the following simulation experiments was to validate the accuracy of the SLRI method for a variety of K values compared to the plain LRI method by means of spectral RMS and colorimetric errors. The Neugebauer primaries were chosen from a Canon (i9900, CMYKRG dye-based) and an Epson (Stylus Pro 5500, CMYKOG pigment-based) printer and are shown in Fig. 3. For the simulation we used all combinations of Yule–Nielsen factors $n=1,2,\ldots,10$ and $K=1,\ldots,N$, where the sampling rate was chosen to be $N=31$.

In Simulation I, in-gamut reflectance spectra were used as input to the SLRI and LRI methods. These spectra were constructed using a YNSN model and the following colorant combinations:

$$\text{Canon:} \quad (C,M,Y,K,R,G)^T \in \{0,0.2,0.4,0.6,0.8,1\}^6, \tag{32}$$

$$\text{Epson:} \quad (C,M,Y,K,O,G)^T \in \{0,0.2,0.4,0.6,0.8,1\}^6. \tag{33}$$

The τ-factor for the termination criteria used by the LRI method (see Section 1.3) was set to $\tau=5\cdot10^{-5}$.

In Simulation II, two multispectral images were used to validate the behavior of the SLRI method dealing with out-of-gamut spectra (see Fig. 4). These images are part of a free available database of multispectral images published on the website of the University of Joensuu, Finland (http://spectral.joensuu.fi/) (cf. Ref. 24). The correlation of neighboring pixels was used to reduce the iteration number. For this purpose the pixels in the images were arranged row-wise, and the separation of the previous pixel was used as start value of the current pixel. The τ-factor was set to $\tau=10^{-4}$.

For both simulations, spectral RMS and colorimetric errors were calculated between the given reflection spectra and the predictions resulting from the LRI or SLRI optimi-

Table 4 Colorimetric results for the Epson printer in Simulation I. For each K, the mean, standard deviation, and maximal ΔE_{00}-values were calculated for all Yule–Nielsen n-values. A K value of 31 is similar to the plain LRI method.

	ΔE_{00}, A			ΔE_{00}, C			ΔE_{00}, F11		
K	Mean	Std	Max	Mean	Std	Max	Mean	Std	Max
1	15.8	9.1	49.8	15.3	8.4	50.5	15.6	8.7	50.8
2	7.9	6.3	41.2	9.2	7.2	49.7	9.0	7.4	46.7
3	2.7	2.5	22.4	2.0	1.8	17.7	2.4	2.3	22.4
4	0.7	0.5	4.7	0.8	0.6	5.9	0.9	0.7	7.5
5	0.6	0.4	5.3	0.6	0.5	5.9	0.8	0.6	8.1
6	0.6	0.4	5.2	0.6	0.5	5.9	0.8	0.6	8.0
7	0.6	0.4	4.3	0.6	0.5	5.9	0.7	0.5	6.8
8	0.6	0.4	4.2	0.6	0.4	5.8	0.7	0.5	6.8
9	0.6	0.4	4.6	0.6	0.4	6.2	0.7	0.5	7.0
10	0.6	0.4	4.7	0.6	0.4	6.2	0.7	0.5	7.3
11	0.6	0.4	4.7	0.6	0.4	6.2	0.7	0.5	7.2
⋮	⋮	⋮	⋮	⋮	⋮	⋮	⋮	⋮	⋮
31	0.6	0.4	4.7	0.6	0.4	6.2	0.7	0.5	7.2

zation. In this article, the spectral RMS difference between two discrete spectra $\vec{x}_1, \vec{x}_2 \in [0,1]^N$ was calculated as follows:

$$\mathrm{RMS}(\vec{x}_1, \vec{x}_2) = \frac{\|\vec{x}_1 - \vec{x}_2\|_2}{\sqrt{N}}. \tag{34}$$

The authors want to reemphasize that the prediction accuracy of the YNSN model in terms of spectral or colorimetric errors is not the subject of this article. The focus of the following simulation experiments is set to the inversion accuracy particularly concerning the used dimension K of the Neugebauer subspace.

4 Results and Discussion

The spectral RMS results of Simulation I are shown in Table 2, where the average iteration numbers are also presented. Some colorimetric results in terms of ΔE_{00} values for the illuminants CIE A (incandescent light), CIE C (average daylight), and CIE F11 (fluorescent lamp) can be found in Tables 3 and 4. Figures 5 and 6 show the RMS accuracy dependent on the Yule–Nielsen n-factor and the Neugebauer subspace dimension K.

The results for in-gamut spectra show that already small K values lead to acceptable accuracy. A mean RMS error smaller than 0.02, a value that is sufficient in various applications,[25] is reached for $K>6$ for both printers, as can

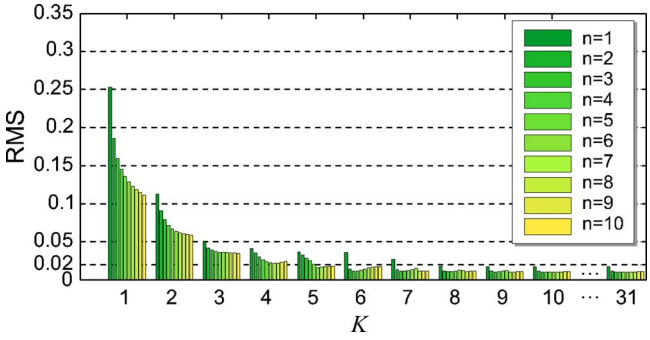

Fig. 5 Mean RMS error dependent on the Yule–Nielsen n-value and the K value for the Canon printer in Simulation I. For $K>7$, there are no major changes in accuracy. A K value of 31 is similar to the plain LRI method.

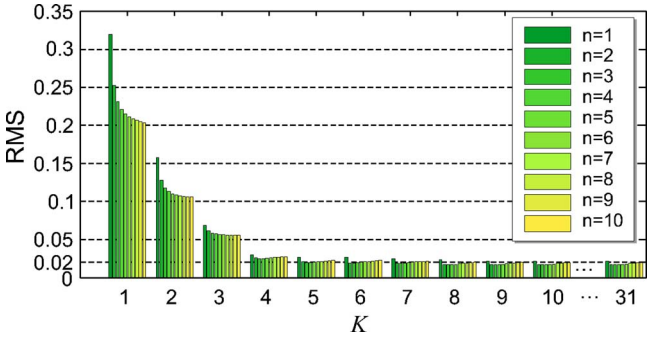

Fig. 6 Mean RMS error dependent on the Yule–Nielsen n-value and the K value for the Epson printer in Simulation I. For $K>8$, there are no major changes in accuracy. A K value of 31 is similar to the plain LRI method.

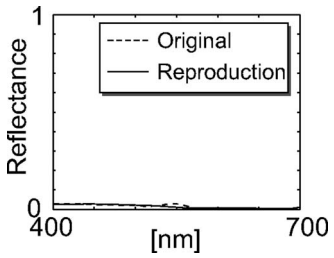

Fig. 7 The given reflectance and the reproduction that produce the ΔE_{00} error of 19.0 for the illuminant CIE F11 (see Table 3). The spectral RMS difference between these reflectances is only 0.031.

be seen from Table 2. This is also reflected in the colorimetric results, which are already smaller than 1 on average for $K \geqslant 6$. The reason for some large maximal colorimetric errors is the behavior of color differences for very dark reflectances. A small difference in reflectance space can result in a large color difference (see Fig. 7). All large colorimetric differences correspond to reflectances near zero. It is widely recognized that when minimizing spectral RMS errors, large colorimetric errors for dark colors can be the consequence.

For $K \geqslant 8$, the mean number of iterations is nearly unchanged. The results of the SLRI method for $K > 8$ are similar to the LRI method. To further decrease the error rates, a smaller τ-value can be selected, leading to additional iterations.

For Simulation II, Table 5 shows the results for the Canon printer and Table 6 those for the Epson printer. As expected, the RMS error rates are significantly higher than in Simulation I because the images contain out-of-gamut reflectances. An implicitly spectral gamut mapping is performed by the SLRI/LRI methods by choosing an in-gamut reflectance with the smallest RMS distance to the given pixel reflectance in $1/n$ space. For practical applications, this kind of spectral gamut mapping often achieves visually poor results and should be replaced by a transformation better related to the human visual system. However, in our experiments we are interested in the minimal number of required dimensions to achieve the same RMS error rates as the LRI method.

In this simulation, as well as in Simulation I, the results validate the mathematical conclusions: For both printers and both images, a significant improvement of RMS error rates cannot be observed for $K > 6$. Also, the number of iterations is stable for these K values and is clearly smaller compared with Simulation I due to utilization of the correlation of neighboring pixels. Finally, in Table 7 we give numerical examples of the mean number of multiplications necessary to invert the YNSN model for a pixel reflectance.

Table 5 RMS results for the Canon printer in Simulation II. For each K, the mean, standard deviation, and maximal RMS error and the average number of iterations were calculated for all Yule–Nielsen n-values. A K value of 31 is similar to the plain LRI method.

	Young Girl				*Fruits and Flowers*			
	RMS			Iterations	RMS			Iterations
K	Mean	Std	Max	Mean	Mean	Std	Max	Mean
1	1.139	0.544	2.355	10.8	0.525	0.386	2.309	10.0
2	0.609	0.308	1.649	12.7	0.257	0.156	1.234	11.7
3	0.178	0.062	0.501	14.5	0.192	0.105	0.687	13.2
4	0.176	0.063	0.501	16.5	0.157	0.086	0.688	20.4
5	0.160	0.054	0.501	17.9	0.150	0.085	0.688	21.9
6	0.151	0.049	0.501	19.1	0.143	0.077	0.671	23.1
7	0.149	0.048	0.499	18.5	0.142	0.076	0.672	22.8
8	0.149	0.048	0.499	18.3	0.141	0.075	0.676	23.1
9	0.149	0.048	0.499	18.2	0.141	0.074	0.679	22.9
10	0.149	0.048	0.500	18.3	0.140	0.074	0.677	23.0
11	0.149	0.048	0.500	18.3	0.140	0.074	0.677	23.0
⋮	⋮	⋮	⋮	⋮	⋮	⋮	⋮	⋮
31	0.149	0.048	0.500	18.3	0.141	0.074	0.677	23.0

Table 6 RMS results for the Epson printer in Simulation II. For each *K*, the mean, standard deviation, and maximal RMS error and the average number of iterations were calculated for all Yule–Nielsen *n*-values. A *K* value of 31 is similar to the plain LRI method.

	Young Girl				*Fruits and Flowers*			
	RMS			Iterations	RMS			Iterations
K	Mean	Std	Max	Mean	Mean	Std	Max	Mean
1	0.770	0.405	2.12	11.0	0.409	0.365	2.237	10.1
2	0.295	0.217	1.44	12.3	0.288	0.200	1.100	11.7
3	0.188	0.067	0.460	13.6	0.230	0.147	0.793	14.6
4	0.156	0.058	0.445	21.9	0.221	0.147	0.785	21.1
5	0.120	0.041	0.265	25.5	0.203	0.143	0.782	20.4
6	0.120	0.041	0.264	25.5	0.203	0.143	0.783	20.5
7	0.119	0.040	0.266	25.2	0.203	0.143	0.783	20.7
8	0.118	0.040	0.267	25.9	0.202	0.142	0.783	21.3
9	0.118	0.040	0.267	25.9	0.202	0.142	0.783	21.4
10	0.118	0.040	0.267	25.9	0.202	0.142	0.783	21.5
11	0.118	0.040	0.267	25.8	0.202	0.142	0.784	21.5
⋮	⋮	⋮	⋮	⋮	⋮	⋮	⋮	⋮
31	0.118	0.040	0.267	25.9	0.202	0.142	0.784	21.4

Table 7 Numerical examples of the mean number of multiplications that were necessary to invert the YNSN model for a pixel reflectance

Printer (*Image*)	SLRI (*K*=7)	LRI
Canon (*Young Girl*)	9,245	37,918
Canon (*Fruits and Flowers*)	11,343	47,656
Epson (*Young Girl*)	12,515	53,665
Epson (*Fruits and Flowers*)	10,319	44,341

The experiments show that minor revisions of the LRI method can significantly reduce the computational effort without changing the inversion accuracy.

5 Conclusion

We have shown how simple revisions of the linear regression iteration (LRI) method to invert the Yule–Nielsen spectral Neugebauer (YNSN) model can significantly reduce the computational complexity without changing the inversion accuracy. This new technique, the subspace linear regression iteration (SLRI) method, uses the length-preserving properties of unitary matrices and the low effective dimension of spectral printer gamuts to perform the

iterations within the Neugebauer subspace. Simulation experiments using two six-colorant printers showed the SLRI to have a mean reduction of multiplication operations of over 70% compared to the LRI while retaining inversion accuracy.

Acknowledgment

The authors thank the Deutsche Forschungsgemeinschaft (German Research Foundation) for sponsorship of this project.

Appendix: Example of the YNSN Model Decomposition in $1/n$ Space

The YNSN model of a CMY printer can be decomposed for cyan in $1/n$ space according to Eqs. (6), (10), and (11) as follows:

$$\vec{R}(\psi_c,\psi_m,\psi_y)=\vec{A}_C(\psi_m,\psi_y)\psi_c+\vec{B}_C(\psi_m,\psi_y) \tag{35}$$

$$=A_C\vec{v}_C(\psi_m,\psi_y)\psi_c+B_C\vec{v}_C(\psi_m,\psi_y), \tag{36}$$

where the matrices A_c and B_c and the vector $\vec{v}_c$ can be stated as

$$A_c=\begin{bmatrix}(-R_{1,\lambda}^{1/n}+R_{2,\lambda}^{1/n})^T\\(R_{1,\lambda}^{1/n}-R_{2,\lambda}^{1/n}-R_{3,\lambda}^{1/n}+R_{4,\lambda}^{1/n})^T\\(R_{1,\lambda}^{1/n}-R_{2,\lambda}^{1/n}-R_{5,\lambda}^{1/n}+R_{6,\lambda}^{1/n})^T\\(-R_{1,\lambda}^{1/n}+R_{2,\lambda}^{1/n}+R_{3,\lambda}^{1/n}-R_{4,\lambda}^{1/n}+R_{5,\lambda}^{1/n}-R_{6,\lambda}^{1/n}-R_{7,\lambda}^{1/n}+R_{8,\lambda}^{1/n})^T\end{bmatrix}^T, \tag{37}$$

$$B_c=\begin{bmatrix}(R_{1,\lambda}^{1/n})^T\\(-R_{1,\lambda}^{1/n}+R_{3,\lambda}^{1/n})^T\\(-R_{1,\lambda}^{1/n}+R_{5,\lambda}^{1,n})^T\\(R_{1,\lambda}^{1/n}-R_{3,\lambda}^{1/n}-R_{5,\lambda}^{1/n}+R_{7,\lambda}^{1/n})^T\end{bmatrix}^T,$$

$$\vec{v}_c(\psi_m,\psi_y)=\begin{bmatrix}1\\\psi_m\\\psi_y\\\psi_m\psi_y\end{bmatrix}. \tag{38}$$

In a similar manner, the YNSN model can be decomposed for magenta and yellow.

References

1. ICC. *File Format for Color Profiles*. http://www.color.org, 4.0.0 edition (2002).
2. M. R. Rosen and M. W. Derhak, "Spectral gamuts and spectral gamut mapping," in *Spectral Imaging: Eighth International Symposium on Multispectral Color Science* **6062**, San Jose, CA, SPIE (2006).
3. M. W. Derhak and M. R. Rosen, "Spectral colorimetry using LabPQR—an interim connection space," *J. Imaging Sci. Technol.* **50**, 53–63 (2006).
4. S. Tsutsumi, M. R. Rosen, and R. S. Berns, "Spectral reproduction using LabPQR: Inverting the fractional-area-coverage-to-spectra relationship," in *ICIS*, Rochester, NY, IS&T, pp. 107–110 (2006).
5. D. R. Wyble and R. S. Berns, "A critical review of spectral models applied to binary color printing," *Color Res. Appl.* **25**, 4–19 (2000).
6. H. E. J. Neugebauer, "Die theoretischen Grundlagen des Mehrfarbenbuchdrucks," *Zeitschrft für wissenschaftliche Photographie, Photophysik und Photochemie*, **36**, 73–89 (1937) [reprint in Ref. 26, translation in Ref. 27].
7. J. A. C. Yule and W. J. Nielsen, "The penetration of light into paper and its effect on halftone reproduction," *TAGA Proceedings*, 65–76 (1951).
8. J. A. C. Yule and R. S. Colt, "Colorimetric investigations in multicolor printing," in *TAGA Proceedings*, pp. 77–82 (1951).
9. J. A. S. Viggiano, "The color of halftone tints," in *TAGA Proceedings*, pp. 647–661 (1985).
10. J. A. S. Viggiano, "Modeling the color of multi-color halftones," in *TAGA Proceedings*, pp. 44–62 (1990).
11. S. Zuffi and R. Schettini, "Spectral-based printer characterization," in *CGIV*, Poitiers, France, IS&T, pp. 598–602 (2002).
12. L. A. Taplin, "Spectral modeling of a six-color inkjet printer," MSc thesis, RIT, Rochester NY (2001).
13. D.-Y. Tzeng, "Spectral-based color separation algorithm developed for multiple-ink color reproduction," PhD thesis, RIT, Rochester, NY (1999).
14. D.-Y. Tzeng and R. S. Berns, "Spectral-based six-color separation minimizing metamerism," in *IS&T/SID*, Scottsdale, AZ, pp. 342–347 (2000).
15. P. Urban and R.-R. Grigat, "Spectral-based color separation using linear regression iteration," *Color Res. Appl.* **31**, 229–238 (2006).
16. R. Rolleston and R. Balasubramanian, "Accuracy of various types of Neugebauer model," in *IS&T/SID*, Scottsdale, AZ, pp. 32–36 (1993).
17. J. S. Arney, "A probability description of the Yule–Nielsen effect," *J. Imaging Sci. Technol.* **41**, 633–636 (1997).
18. J. S. Arney and M. Katsube, "A probability description of the Yule–Nielsen effect II: The impact of halftone geometry," *J. Imaging Sci. Technol.* **41**, 637–642 (1997).
19. J. S. Arney and S. Yamaguchi, "The physics behind the Yule–Nielsen equation," *PICS: Image Processing, Image Quality, Image Capture, Systems Conf.*, pp. 381–385 (1999).
20. G. L. Rogers, "Optical dot gain in a halftone print," *J. Imaging Sci. Technol.* **41**, 643–656 (1997).
21. K. Iino and R. S. Berns, "Building color-management modules using linear optimization I. Desktop color system," *J. Imaging Sci. Technol.* **42**, 79–94 (1998).
22. H. J. Trussel and M. S. Kulkarni, "Sampling and processing of color signals," *IEEE Trans. Image Process.* **5**, 677–681 (1996).
23. P. E. Gill, W. Murray, and M. H. Wright, *Practical Optimization*, Academic Press, New York, (1981).
24. O. Kohonen, J. Parkkinen, and T. Jaaskelainen, "Databases for spectral color science," in *AIC Colour 05*, Granada, Spain, pp. 1649–1652 (2005).
25. M. R. Rosen, E. F. Hattenberger, and N. Ohta, "Spectral redundancy in a six-ink ink jet printer," *J. Imaging Sci. Technol.* **48**, 194–202 (2004).
26. H. E. J. Neugebauer, "Die theoretischen Grundlagen des Mehrfarbenbuchdrucks," in *Proceedings of SPIE: Neugebauer Memorial Seminar on Color Reproduction*, 1184, 194–202 (1989).
27. H. E. J. Neugebauer, "The theoretical basis of multicolor letterpress printing," (translated by D. Wyble and A. Kraushaar), *Color Res. Appl.* **30**, 322–331 (2005).

Philipp Urban received his MS in mathematics from the University of Hamburg in 1999 and his PhD in color science from Hamburg University of Technology in 2005. From 1999 until 2006, he was part of the "Vision Systems" research group at Hamburg University of Technology and worked for Ratio Entwicklungen GmbH (ICC-member), where he developed color managing systems. Since 2006 he has been a visiting scientist at the Munsell Color Science Laboratory at the Rochester Institute of Technology. His research interests include color science and multispectral imaging.

Mitchell R. Rosen received his BS from Tufts University in 1984 and his PhD from Rochester Institute of Technology in 2003. He is a research professor in the Center for Imaging Science at the Rochester Institute of Technology. He is also chair of the Digital Cinema program in the School of Film and Animation. He performs research primarily with the Munsell Color Science Laboratory and the Visual Perception Laboratory. His research areas include color management, spectral imaging systems, museum imaging, and eye movement analysis. He teaches graduate courses on color systems and tutorials on color management, color reproduction, and spectral imaging. He is color imaging editor of IS&T's *Journal of Imaging Science and Technology* and is active in organizing international conferences on spectral imaging. His Website is http://www.cis.rit.edu/rosen, and he can be reached at rosen@cis.rit.edu.

Roy S. Berns is the Richard S. Hunter Professor in Color Science, Appearance, and Technology at the Munsell Color Science Laboratory and Graduate Coordinator of the Color Science MS and PhD programs within the Center for Imaging Science at the Rochester Institute of Technology. He received his BS and MS degrees in textile science from the University of California at Davis in 1976 and 1978 and his PhD degree in chemistry from Rensselaer Polytechnic Institute in 1983. His research includes spectral-based imaging, archiving, and reproduction of cultural heritage; spectral modeling of multi-ink printers; quantifying the optical properties of painting varnishes and the impact on appearance, colorant selection for inpainting, and colorimetry.